Study on Sintering Mechanism and Mechanical Properties of Nano-Cu based on Molecular Dynamics Simulation

Qian, Cheng; Hu, Dong; Liu, Xu ; Fan, Xuejun; Zhang, Guoqi; Fan, Jiajie

Study on Sintering Mechanism and Mechanical Properties of Nano-Cu based on Molecular Dynamics Simulation

Cheng Qian[1#], Dong Hu[2#], Xu Liu[1], Xuejun Fan [4], Guoqi Zhang [1,2], Jiajie Fan [1,2,3*]

1 Institute of Future Lighting, Academy for Engineering & Technology; Shanghai Engineering Technology Research Center for SiC Power Device, Fudan University, Shanghai 200433, China
2 EEMCS Faculty, Delft University of Technology, Delft, the Netherlands
3 Research Institute of Fudan University in Ningbo, Ningbo 315336, China
4 Department of Mechanical Engineering, Lamar University, Beaumont, TX, USA
[#]Cheng Qian and Dong Hu equally contribute to present work
*Corresponding: Jiajie Fan (Fudan University), Email: jiajie_fan@fudan.edu.cn

Abstract

Nano-metal materials sintering has received increasing attention in recent years for its promising performance in the wide bandgap semiconductor packaging. In this paper, molecular dynamics (MD) simulation method were applied to simulate the nano-Cu sintering mechanism and the subsequent mechanical behavior. Hybrid sintering, comprising nanosphere (NS) and nanoflake (NF), was carried out at temperatures ranging from 500K to 650K. Furthermore, shearing simulations were conducted with constant strain rates on the sintered structure at multiple temperatures, and subsequently correlated the extracted mechanical properties with the sintering behavior. The results indicated that the mechanical properties of nano-Cu sintered structure were improved by tuning material composition and increasing the sintering temperature. We established a relationship between the sintered microstructure and mechanical response, the shear modulus and shear strength of the sintered structure with NF particles increased to 41.2GPa and 3.51GPa respectively. It offers valuable insights into the preparation phase of nano Cu paste for sintering technology.

Keywords: Nano Cu sintering; molecular dynamics simulation; Nanoflake; Shearing simulation

1. Introduction

The wide-bandgap (WBG) semiconductors represented by SiC and GaN have wide application in many strategic industries, such as renewable energy technology, high-speed railways, intelligent vehicle, and are rapidly developing towards higher power density, higher operating temperature, more functionalization and miniaturization [1, 2]. In order to ensure the reliability and functionality of WBG semiconductor package, a low process temperature joining technology with great stability at high temperature is urgently needed.

Sintering of nano-metal materials offers numerous benefits, such as improved electrical interconnection, mechanical support, and heat dissipation channels for WBG power module packaging. Furthermore, it leverages the nano size effects to achieve "low temperature packaging, high temperature operation" [3]. Compared to nano-Ag, nano-Cu paste has higher melting point, lower material cost, excellent thermal conductivity, and matching thermal coefficient of expansion, which is expected to become the interconnection material for the next generation of high-power electronic packaging [4-6].

Recently, it is reported that the addition of NF can effectively reduce the porosity of sintered structure by promoting the sintering rate and sintering neck growth [7-11]. Unlike sphere-shape nanoparticle, the NF particles are found to continuously deform during the sintering process [12]. Dislocations caused by deformation generate stress inside the particle, and the stress releasing promotes the sintering process.

However, the relationship between particle geometry, sintering condition and the microstructure evolution during Cu sintering has been rarely reported. Li [13] simulated and analyzed the Ag sintering mechanism with addition of Ag NF. Cheng [14] studied the sintering of a multi-particle Cu NPs system at multiple temperatures and pressures. Additionally, simulation efforts have been made to connect the sintered structure with mechanical properties. Hu [15] studied the sintering dynamics of pressure-assisted Cu NPs, and subsequently simulated tensile strength through a uniaxial tension at a constant strain rate.

The present study employs the MD method to simulate the sintering of two Cu nanoparticles and investigates their mechanical behavior. Emphasis is placed on analyzing the sintering kinetics and microstructure evolution of multi-models comprising equal/non-equal dimension Cu nanospheres and nanoflakes to determine the effect of geometry on the sintering process. Simulations were conducted at various sintering temperatures (ranging from 500K to 650K) to identify the dominant sintering mechanism in each model. Additionally, the mechanical behavior was analyzed using constant rate shearing simulation. This research successfully integrates the process temperature, sintered structure, and further mechanical response, demonstrating the methodology's potential for determining material and process conditions for future nano-Cu sintering technology.

2. Methods and modeling

2.1 Atomistic model

In this study, the classical embedded atom method (EAM) potential developed by Adam [16] is used to describe the interaction between Cu atoms. This potential has been proved to be able to accurately describe Cu

inter-atommic properties [17, 18]. The total energy of the system based on this force field is:

$$E_i = F_\alpha\left(\sum_{j\neq i}\rho_\beta\left(r_{ij}\right)\right)+\frac{1}{2}\sum_{j\neq i}\varphi_{\alpha\beta}\left(r_{ij}\right) \qquad (1)$$

Wherein, α and β are the element types of atoms i and j. F is the embedded energy and φ is the pairwise interactions, which are a function of the atom types α and β and the atomic spacing r_{ij}.

As shown in Figure 1, two kinds of sintering structures were constructed in the sintering simulation, namely, the nanosphere(NS)-nanosphere(NS) model and the nanosphere(NS)-nanoflake(NF) model, to investigate the effect of different particle size ratios (1:1-1:3) and the addition of NF on sintering. The diameter of NS was set to 5nm, 10nm, and 15nm. The length of NF particles was set to 5nm and 10nm, length-to-thickness ratio is 5:2. In order to eliminate the influence of model orientation, all components were initially set at <100> orientation. In addition, 3.6 Å is taken as the initial spacing between pair of particles, which is the value of the Cu lattice constant.

In this study, the molecular dynamic simulation was carried out in Large-scale Atomic/Molecular Massively Parallel Simulator (LAMMPS) [19]. The simulation results were visualized in Open Visualization Tool (OVITO) [20].
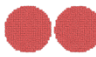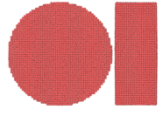

The details of atomistic model include the atom numbers and configurations.			
	NS1-NS1 model(1:1)	NS1-NS2 model(1:2)	NS1-NS3 model(1:3)
NS-NS Model			
Atom numbers	11150	50084	155754
	NS1-NF1 model	NS2-NF2 model	
NS-NF Model			
Atom numbers	9680	77823	

Figure 1. The details of atomistic model.

2.2 Simulation flow

All simulations are carried out in a three-dimensional simulation box with periodic boundaries with a time step of 1 fs. NVT ensemble was adopted for the sintering simulation. The entire simulation profile is shown in Figure 2. Prior to the system assembly, the NS and NF were relaxed at the sintering temperature within 50 ps to obtain the equilibrium status.
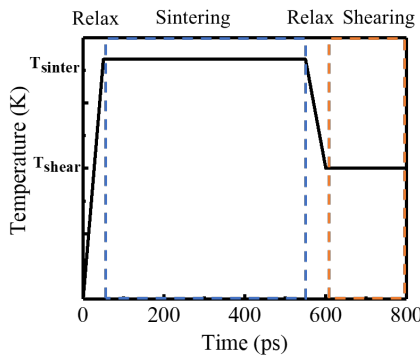

Figure 2. Nano-Cu shear simulation process.

Before the sintering simulation, the system energy was at first minimized through the steepest descent algorithm. Afterwards, the entire model was simulated for 500 ps at sintering temperature T_{sinter} to ensure a post-sintering equilibrium status. A relaxation step follows the sintering process, bringing the entire model back to the shearing temperature T_{shear}. Subsequently, the shearing simulation was done within 200 ps.

2.3 Sintering simulation

In the sintering simulation, Considersing the practical sintering temperture adopted in the reported studies, 500K, 550K, 600K and 650K were consdierately selected as the sintering simulation temperature.

The sintering process was evaluated by the total dislocation length, lattice transformation, and the geometry evolution. In this study, dislocation analysis (DXA) and common neighbor analysis (CNA) were used to characterize the sintered microstructures. Besides, the ratio of the neck size (x) to the dimension of the particles (W) is defined as x/W, shown in Figure 3. In order to obtain the size of the neck, a dynamically distributed block with a thickness of 3.5Å is defined in the neck region, which contains less than 3 layers of nano-Cu atoms. MSD was also employed to evaluate the sintering mechanism of the entire model and to determine the rate of diffusion. The calculation formula is as follows:

$$\mathrm{MSD} = \frac{1}{N}\sum_{i=1}^{N}\left[r_i\left(t\right)-r_i\left(0\right)\right]^2 \qquad (2)$$

Where N is the number of atoms, $r_i(t)$ and $r_i(0)$ are the positions of atom i at time t and time 0, respectively.
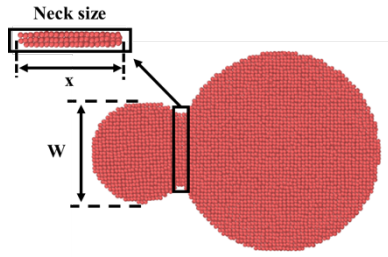
Figure 3.NS-NS model and geometric parameters for the sintering simulation.

2.4 Shearing simulation

To evaluate the adhesive strength of each sintered structure, shearing simulation with variable temperature were further carried out on the sintered model with a constant strain rate. In this simulation, 300K, 450K and 600K were chosen to simulate the mechanical resposnse to the different shearing temperature. Two baseplates were added to implement the shearing simulation as shown in Figure 4. The upper plate was used to apply a constant speed of 0.2 Å/fs along the <100> direction. In the contrast, tthe lower plate was applied to fix the position of the model. The length of the upper and lower substrates is twice the diameter of the larger component and the thickness was set as 1 nm.
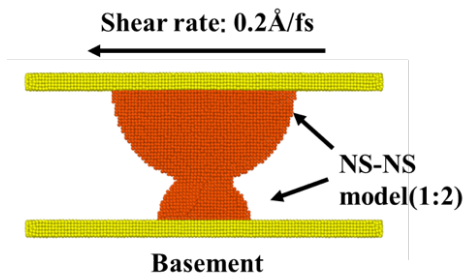

Figure 4.NS-NS model and geometric parameters for the shearing simulation.

The stress-strain curve of the sintered region is obtained in the shear simulation. The monoatomic stress tensor of the sintered Cu atoms was given by the following formula:

$$S_{ab} = -mv_a v_b - W_{ab} \qquad (3)$$

Where a and b take on values x, y, z to generate the components of the tensor. The first term is a kinetic energy contribution and W_{ab} is the virial contribution.

In order to eliminate the influence of volume term, it is generally to sum the component of monatomic stress and then divide it by the volume of the sintered region:

$$\sigma = \frac{1}{N} \sum_{i=1}^{N} \left(\frac{p_i \div v_i}{-10000} \right) \qquad (4)$$

where σ Is the average stress value of the sintered region, N is the number of atoms, p is the calculated value of the i_{th} atom, and v is the volume term of the i_{th} atom.

In addition, shear fracutre in a FCC metal takes place along the close-packed plane, as 45° to shearing direction.

Thus, the *XZ* stress tensor component was adopted to derive the stress.

3. Simulation results and discussion

3.1 Sintering simulation

3.1.1 Effect of geometry on the sintering

Figures 5(a)-(b) and 6(a)-(b) show the evolution in total dislocation length and HCP ratio during the 500K sintering of the NS-NF model and the NS-NS model. The details in the blue frames were zoomed in and placed aside. It can be seen that the whole sintering process was divided into several stages according to the dislocation behavior, as shown in Figure.5(c) and Figure 6(c).

In the first stages, the two components approach to each other and resulting in no change in either dislocation length or the HCP ratio. Afterwrads, the dislocation length of the NF-NS model starts to rapidly increase at state <2> (6ps). However, it takes place in a NS-NS model at 26 ps. It can be figured out in Figure 5(a), a small necking region formed at this step with minor dislocations and HCP crystal structures generated in the neck region. Then, the neck grows rapidly and the dislocations increase continuously, producing a small number of HCP atoms in state <3>, and the dislocation reaches its maximum in state <4>, however, far more dislocations are generated in the NS-NF model than in the NS-NS model. It can be attributed that the NF was bent towards the NS during sintering, and more dislocations were generated to accommodate the deformation.

With the further growth of the neck, the dislocation gradually dispeared and the HCP crystal atoms are accordingly transformed into FCC crystal atoms, as shown in Figure 5(a) <5>. The NF is less bent compared to the previous stages. However, due to the presence of residual stress in the sintered structure, the NF tilted slightly and the NP rotated to the proper orientation to dissipate the energy, resulting in new dislocations. Subsequently, dislocations move under the action of internal stress and generate stacking faults in the direction of stress.

As the length of the neck region stablizes, the dislocations annihilates at the surface according to the unreservable plastic deformation. Finally, after 45 ps, the total dislocations length and the HCP ratio slightly fluctuates, indicating the sintering process enters the equilibrium phase.

Fig. 6 (c) depicts the sintering process of the NS-NS model. Unlike the dislocation of the NS-NF model did not vanish completely, the NS-NS model results in a relatively low dislocation length. It can be caused by the participation of the NF, which tilts during the sintering simulation. Therefore, a part of the particles continue to be sintered, leaving stacking faults crossing the NS and the NF.

Figure 5. Evolution of (a)total dislocation length and (b)HCP ratio during sintering; (c) Snapshots of NS-NF during sintering :Lattice structures, HCP lattice structure and dislocations.

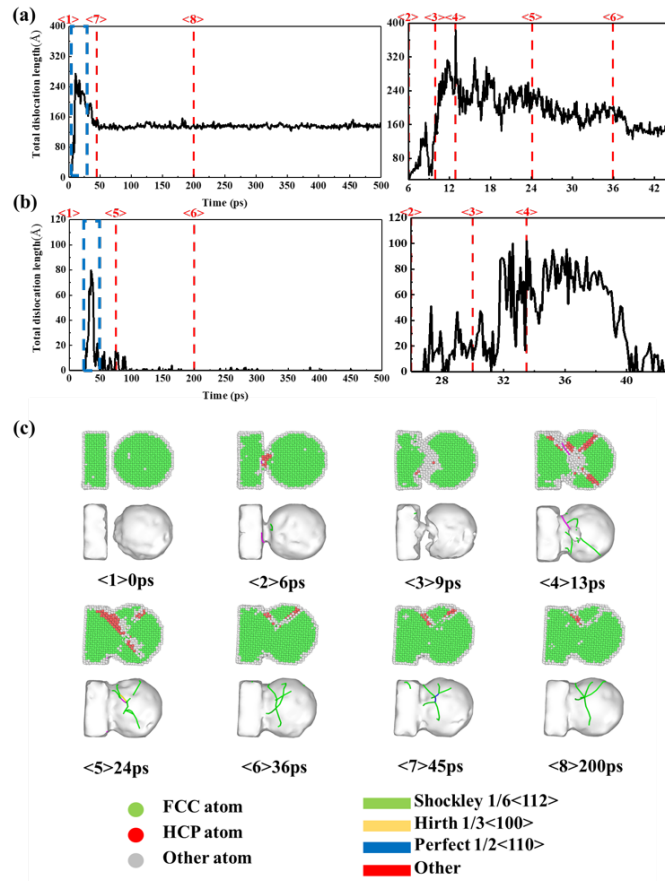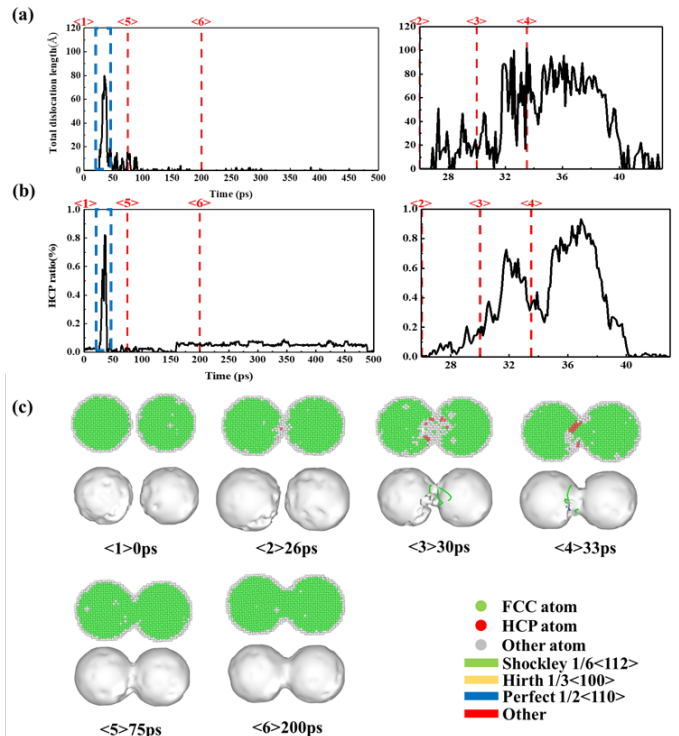*Figure 6. Evolution of (a)total dislocation length and (b)HCP ratio during sintering; (c) Snapshots of NS-NS during sintering :Lattice structures, HCP lattice structure and dislocations.*

To further investigate influence factors of geometries and size ratio, the evolution of x/W and MSD on the NS-NS models and NS-NF models were ploted in Figure 7. It can be seen that the non-equal diameter NS-NS models obtain a larger necking region than the equal diameter NS-NS model. However, tuning the particle size has limited effect on the improvement of sintered neck length from the results of NS1-NS1 and NS1-NS2 model. Besides, the x/W of the NS-NF model present better performance than NS-NS models with the same dimension. The x/W of the NF-NP model is 1.2 times higher than that of the NS-NS model. It proves that the participation of NF particles significantly improves the sintering neck size.

The sintering mechanism of different models was also investigated by MSD, as shown in Figure 7 (b). the slope of the MSD curve is proportional to the diffusion rate, and the rapid increase of MSD in the initial stage contributes to plastic deformation.The presence of the NF not only accelerates the diffusion rate of atoms, but also makes the plastic flow between Cu NPs more intense, which is the reason why the neck size of the NF-NS model is larger than that of the NS-NS model.

As a result, it can be concluded that: (1) the non-equal diameter NS-NS model has a larger sintering neck size than the equal diameter NS-NS model; (2) the NS-NF model can greatly promote the sintering performance compared to the equal diameter NS-NS models. (3) The presence of NF enhanced plastic deformation during sintering by promoting atomic diffusion on the surface and volume of the particles as well as generating more defects. The stress release caused by these defects promoted the sintering of the nanoparticles.
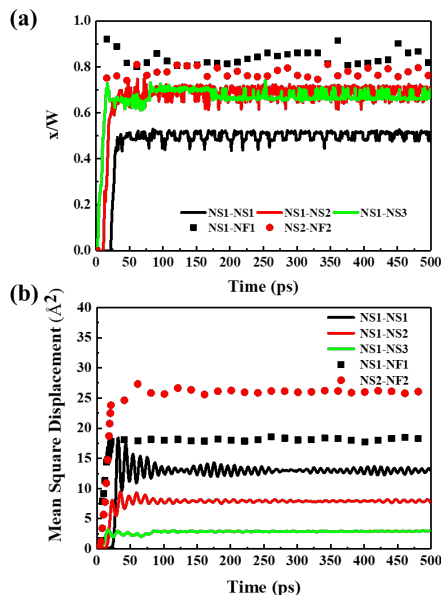

Figure 7. (a) The x/W at 500K sintering temperature for different models; (b) MSD at 500K sintering temperature for different models.

3.1.2 Effect of temperature on the sintering

In this section, various temperatures were applied on NS1-NS1 model and NS1-NF1 model. Figure 8 plots x/W curve as a function of sintering time at different sintering temperatures. Compared with the NS-NF model, the sintered neck growth of the NS-NS model is more sensitive to the sintering temperature. Higher sintering temperature results in a larger x/W ratio. In contrast, the neck size of NS-NF model remain stable according to the increased temperature. The difference on the temperature dependence implies that the sintering process of NS-NF model is less dominated by the surface diffusion, where sintering temperature plays an essential role.
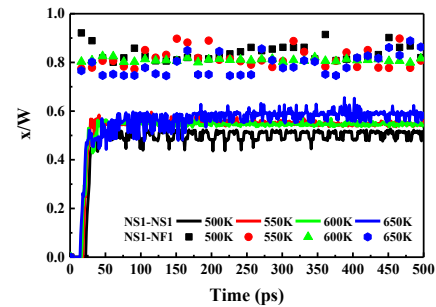

Figure 8. x/W for NS-NS and NS-NF models at different sintering temperatures.
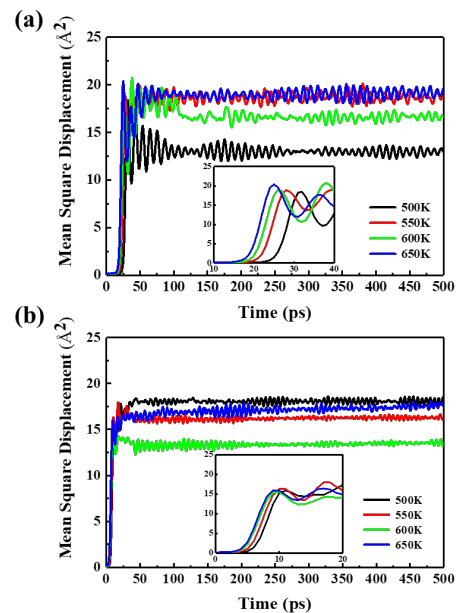
Figure 9. (a) MSD of NS1-NS1 model at different temperatures.; (b) MSD of NS1-NF1 model at different temperatures.

The results can also be verified by the MSD of NS-NF and NS-NS models at different temperatures shown in Figure 9. In NS-NS model, improving sintering temeprature presents significant promotion in the MSD. Also, the slope in the rapid increase stage also indicate a higher diffusion rate at the higher temperature. It suppose that the sintering in the NS-NS model is mainly driven by the surface diffusion. In the contrast, the MSD rapid stage in the NS-NF model ends at 10 ps, but the x/W ratio still keeps growing, which indirectly proves that the mass

migration is mainly contributed by the plastic flow instead of the surface diffusion at this time. Meanwhile, the slope of the NS-NF model was larger than that of the NS-NS model.

3.2 Shear simulation

3.2.1 Microstructure analysis of shear simulations

Shear simulation was further demonstrated on the post-sintered atomistic model. Considering the practical experimental condition, the shearing tests were simulated at 300 K. Figure 10 shows the stress-strain curves and dislocation length evolution of NS1-NS2 model sintered at 500 K. Moreover, the whole shear process is divided by six key time points according to the stress evolution. Figure 11 shows the model snapshots at each time point. The results show that the sintered NS1-NS2 model can withstand a shear stress close to 1.5 GPa. A small stress concentration can be noticed in the neck region before shear, which is attributed to the residual SF from sintering. In the shear simulation, the stress rises rapidly with the increase of strain at the beginning at state <1>, and the model is in the elastic stage at this time. Then the stress-strain curve follows Hooke's law, the curve of the elastic stage is fitted, and its slope can be regarded as the shear modulus of the sintered model. Subsequently, the sintered model enters the yield phase, and the stress fluctuates up and down with increasing strain, as in states <2>-<4>. At this stage, the dislocation length first decreases and then increases. Meanwhile, it is found that the dislocation direction in the model changes from northwest to northeast. This is owing to the fact that during the shear

process, dislocations generated during sintering are constantly disassembled and new dislocations are formed under the action of shear stress. Finally, the sintered structure enters the viscoplastic deformation stage, and the stress decreases continuously with the increase of strain until it tends to 0. The maximum stress in the critical fracture phase of the nano-Cu sintered structure is the shear strength.

From state <2> to state <6>, the neck of Cu NPs shrinks continuously with the movement of the upper basement, and a serrated evolution of stress was observed. It is because the dislocations nucleated , propagate and eventually decompose to achieve plastic deformation. This dislocation behavior continuously takes place under the objected external force, leading to structural instability.
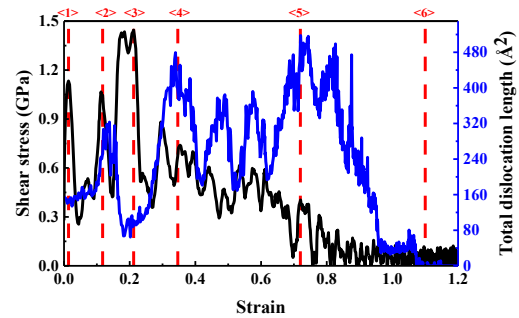

Figure 10. Shear stress and total dislocation length in NS1-NS2 shear simulation.
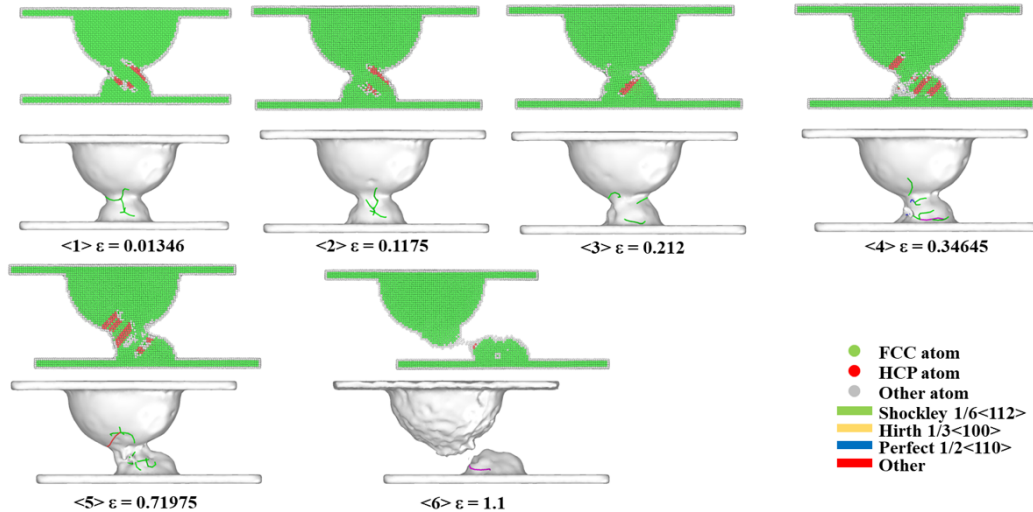

Figure 11. Snapshots of NS1-NS2 model during sintering :Lattice structures, HCP lattice structure and dislocations.

3.2.2 Effects of process parameters on the mechanical properties

The stress-strain curves of NS-NS and NS-NF model at different shear temperatures are shown in Figures 12(a) and (b). After entering the yield stage, the curves fluctuate greatly during the plastic deformation process. The model structure is more complex in this stage. The structure

changes with the increase of dislocation activity, and the sintering neck area changes significantly. It can be seen that the shear strength and shear modulus decrease with the increase of shearing temperature. The shear strength of the NS1-NS1 model is 2.47Gpa at 600 K, which is lower than that of the value extracted at 300K shearing temperature. The shear strength is significantly improved

after adding the NF particles. At 600K shear temperature, the shear strength is increased by 25%, reaching 3.04GPa.

From Figure 13, It can be seen that increasing the sintering temperature of the NS1-NS1 model to 650K increases the shear strength and shear modulus. The larger the neck size, the better the shear modulus and shear strength of the sintered structure. At the same time, Figure 14 also presents the stress-strain curves of different initial models. NS1-NF1 model results in the outperformed mechanical properties. When the size of sintered particles increases, the shear strength of NS2-NF2 model decreases compared with NS1-NF1 model. It is conjectured that the diffusion mechanism and plastic mechanism are not sufficient to promote further sintering of large size particles at 500K, and incomplete sintering leads to a decrease in mechanical properties. It is also observed that the shear stress variation of non-equal dimension NS-NS model is more significant. It can be caused by the model size that the stress derived from a small paricle can be affected more by the dislocation activity.
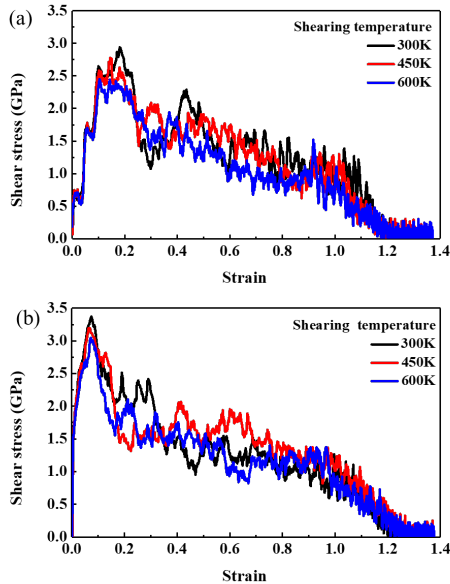

Figure 12. (a) Shear stress in NS1-NS1 at different shearing temperatures; (b) Shear stress in NS1-NF1 at different shearing temperatures.
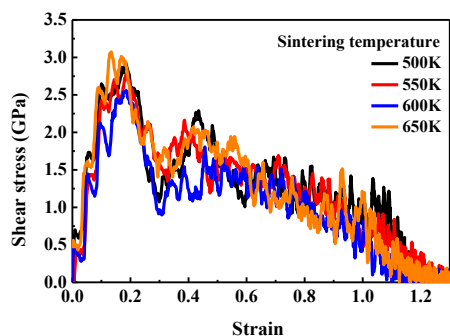

Figure 13. NS1-NS1 shear simulation of shear stress at different sintering temperatures.
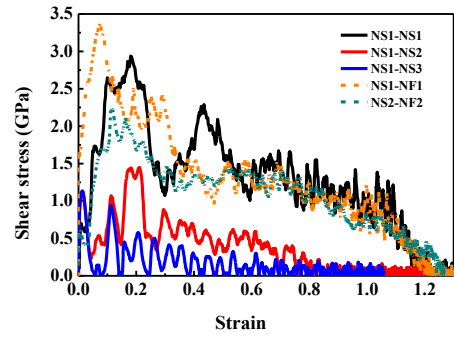

Figure 14. Shear stress of different sintered structures at 500K sintering temperature.
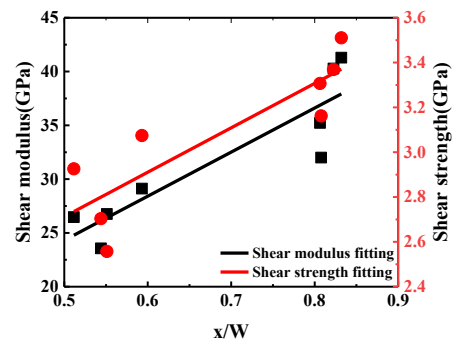

Figure 15. Shear modulus and Shear strength of the sintered structure with different x/W.

Furthermore, to bridge the sintering performance to the mechnical response, Figure 15 plots the shearing modulus and shear strength as a function of the sintering perfomance, x/W. It can be found that the mechanical behavior of the sintered model are highly consistent with the above sintering results. The fitting of shear modulus and shear strength shows that both increase linearly with x/W. Larger x/W leads to a stronger shearing performance.

The effect of addition of NF on the interconnection of Cu NPs is more significant than that of temperature. The results show that larger x/W, that is, larger neck size, indicates better model sintering quality. Under the same size, the NS-NF model has better mechanical properties than the NS-NS model. The model in which NF was added sintering at 500K has a shear strength of 3.51GPa, which is much greater than that of the NS-NS model at the same sintering temperature. The mechanical properties of nano-Cu sintered structure were also improved by increasing the sintering temperature. However, the effect of temperature change is less significant than that caused by the change of sintering structure of NF particles. In general, structures with larger x/W have better shear modulus and shear strength.

4. Conclusions

This paper presents a EAM based molecular dynamics simulation study to investigate the sintering behavior and mechanism of Cu NPs. Considering the geometric structure of sintered materials, 5 hybrid models comprising equal/non equal NS-NF and NS-NS pair was established and subsequently simualted at multiple

sintering temperatures. The evolution of x/W and MSD were recorded to evaluate the sintering process. In addition, dislocation activity were used to analyze the atomic migration behavior during sintering; Eventually, shearing simulation was conducted on the sintered structure at multiple shearing temperature.

The results show that: (1) The influence of hybrid composition on the growth of neck region was more significant than that of sintering temperature. Increasing the diameter ratio can promote the atomic diffusion of the particles and promote the growth of the sintering neck. Compared with the equal dimension NS-NS model, the NS-NS models with diameter ratios of 1:2 and 1:3 had larger x/W; (2) The NS-NF model resulted in a larger x/W and MSD, indicating better sintering performance. It was revealed that the NF deformed towards the neck region, and the increased contact area further improved the growth of the neck region. The stress release generated by the deformation also promotes the sintering of the Cu NPs. In the later stage of sintering, the deformation degree of NF particles decreased and turned to tilt to NS particles; (3) The mechanical properties were reduced at high shearing temperature. However, the shear modulus and shear strength of the sintered structure were enhanced by a larger x/W ratio. The addition of NF promoted the growth of the sintered neck and increased the x/W of the sintered structure, leading to better coalescence of Cu NPs, which also improved the mechanical properties. Compared with the NS1-NS1 model, the shear modulus of the NS1-NF1 model was increased by 41%, approaching 45 GPa, and the shear strength was increased by 14%, reaching 3.51GPa. This result was consistent with experimental results demonstrating that less porous nano-Cu sintered structures exhibit superior mechanical properties. Our study offers theoretical research support for the application of nano-Cu sintered materials in SiC power module packaging.

Acknowledgments

References

1. F. Roccaforte *et al.*, "Emerging trends in wide band gap semiconductors (SiC and GaN) technology for power devices," *Microelectronic Engineering,* vol. 187, pp. 66-77, 2018.
2. R. Khazaka, L. Mendizabal, D. Henry, and R. Hanna, "Survey of high-temperature reliability of power electronics packaging components," *IEEE Transactions on power Electronics,* vol. 30, no. 5, pp. 2456-2464, 2014.
3. H. Yan, P. Liang, Y. Mei, and Z. Feng, "Brief review of silver sinter-bonding processing for packaging high-temperature power devices," *Chinese Journal of Electrical Engineering,* vol. 6, no. 3, pp. 25-34, 2020.
4. Z. Wu, J. Cai, Q. Wang, and J. Wang, "Low temperature Cu-Cu bonding using copper nanoparticles fabricated by high pressure PVD," *AIP Advances,* vol. 7, no. 3, p. 035306, 2017.
5. H. Ji, J. Zhou, M. Liang, H. Lu, and M. Li, "Ultra-low temperature sintering of Cu@ Ag core-shell nanoparticle paste by ultrasonic in air for high-temperature power device packaging," *Ultrasonics sonochemistry,* vol. 41, pp. 375-381, 2018.
6. X. Liu *et al.*, "Microstructural evolution, fracture behavior and bonding mechanisms study of copper sintering on bare DBC substrate for SiC power electronics packaging," *Journal of Materials Research and Technology,* vol. 19, pp. 1407-1421, 2022.
7. J. Nandy, S. Sahoo, and H. Sarangi, "Study on shape dependency of Al-alloy nanoparticles during coalescence in direct metal laser sintering: A molecular dynamics approach," *Materials Today: Proceedings,* vol. 41, pp. 347-351, 2021.
8. J. Yeom *et al.*, "Ag particles for sinter bonding: Flakes or spheres?," *Applied Physics Letters,* vol. 114, no. 25, p. 253103, 2019.
9. C. Wang, G. Li, D. Zhang, and P. Zhu, "Synthesis of triangular silver nanoflakes and its application in die-attachment materials," in *2020 21st International Conference on Electronic Packaging Technology (ICEPT)*, 2020: IEEE, pp. 1-4.
10. S. Soichi and K. Suganuma, "Low-temperature and low-pressure die bonding using thin Ag-flake and Ag-particle pastes for power devices," *IEEE Transactions on Components, Packaging and Manufacturing Technology,* vol. 3, no. 6, pp. 923-929, 2013.
11. H. Zhang, S. Nagao, S. Park, S. Koga, T. Sugahara, and K. Suganuma, "Nano-SiC added Ag paste sintering die-attach for SiC power devices," in *Proceedings of the 5th Electronics System-integration Technology Conference (ESTC)*, 2014: IEEE, pp. 1-4.
12. C. Wang *et al.*, "Low temperature sintered silver nanoflake paste for power device packaging and its anisotropic sintering mechanism," *ACS Applied Electronic Materials,* vol. 3, no. 12, pp. 5365-5373, 2021.
13. S. Li *et al.*, "Sintering mechanism of Ag nanoparticle-nanoflake: a molecular dynamics simulation," *journal of materials research and technology,* vol. 16, pp. 640-655, 2022.
14. B. Cheng and A. H. Ngan, "The sintering and densification behaviour of many copper nanoparticles: A molecular dynamics study," *Computational materials science,* vol. 74, pp. 1-11, 2013.
15. D. Hu, Z. Cui, J. Fan, X. Fan, and G. Zhang, "Thermal kinetic and mechanical behaviors of pressure-assisted Cu nanoparticles sintering: A molecular dynamics study," *Results in Physics,* vol. 19, p. 103486, 2020.
16. J. Adams, S. Foiles, and W. Wolfer, "Self-diffusion and impurity diffusion of fee metals using the five-

frequency model and the embedded atom method," *Journal of Materials Research,* vol. 4, no. 1, pp. 102-112, 1989.

17. L. Wang *et al.*, "New twinning route in face-centered cubic nanocrystalline metals," *Nature communications,* vol. 8, no. 1, p. 2142, 2017.

18. P. Grammatikopoulos, "Atomistic modeling of the nucleation and growth of pure and hybrid nanoparticles by cluster beam deposition," *Current Opinion in Chemical Engineering,* vol. 23, pp. 164-173, 2019.

19. S. Plimpton, "Fast parallel algorithms for short-range molecular dynamics," *Journal of computational physics,* vol. 117, no. 1, pp. 1-19, 1995.

20. A. Stukowski, "Visualization and analysis of atomistic simulation data with OVITO–the Open Visualization Tool," *Modelling and simulation in materials science and engineering,* vol. 18, no. 1, p. 015012, 2009.